

Intracellular Amyloid- β in the Normal Rat Brain and Human Subjects and Its relevance for Alzheimer's Disease

Asgeir Kobre-Flatmoen^{a,b,*}, Thea Meier Hormann^a and Gunnar Gouras^c

^a*Kavli Institute for Systems Neuroscience, Norwegian University of Science and Technology, Trondheim, Norway*

^b*K.G. Jebsen Centre for Alzheimer's Disease, NTNU, Trondheim, Norway*

^c*Department of Experimental Medical Science, Experimental Dementia Research Unit, Lund University, Lund, Sweden*

Accepted 5 July 2023

Pre-press 10 August 2022

Abstract.

Background: Amyloid- β ($A\beta$) is a normal product of neuronal activity, including that of the aggregation-prone $A\beta_{42}$ variant that is thought to cause Alzheimer's disease (AD). Much knowledge about AD comes from studies of transgenic rodents expressing mutated human amyloid- β protein precursor ($A\beta$ PP) to increase $A\beta$ production or the $A\beta_{42/40}$ ratio. Yet, little is known about the normal expression of $A\beta_{42}$ in rodent brains.

Objective: To characterize the brain-wide expression of $A\beta_{42}$ throughout the life span of outbred Wistar rats, and to relate these findings to brains of human subjects without neurological disease.

Methods: $A\beta_{42}$ immunolabeling of 12 Wistar rat brains (3–18 months of age) and brain sections from six human subjects aged 20–88 years.

Results: In healthy Wistar rats, we find intracellular $A\beta_{42}$ ($iA\beta_{42}$) in neurons throughout the brain at all ages, but levels vary greatly between brain regions. The highest levels are in neurons of entorhinal cortex layer II, alongside hippocampal neurons at the CA1/subiculum border. Concerning entorhinal cortex layer II, we find similarly high levels of $iA\beta_{42}$ in the human subjects.

Conclusion: Expression of $iA\beta_{42}$ in healthy Wistar rats predominates in the same structures where $iA\beta$ accumulates and $A\beta$ plaques initially form in the much used, Wistar based McGill-R-Thy1-APP rat model for AD. The difference between wild-type Wistar rats and these AD model rats, with respect to $A\beta_{42}$, is therefore quantitative rather than qualitative. This, taken together with our human results, indicate that the McGill rat model in fact models the underlying wild-type neuronal population-specific vulnerability to $A\beta_{42}$ accumulation.

Keywords: Alzheimer's disease, animal model, disease onset, entorhinal cortex

INTRODUCTION

Amyloid- β ($A\beta$) is a small peptide and a normal product of neuronal activity [1–4]. Several variants of $A\beta$ exist, and all result from sequential enzymatic cleavage of the amyloid- β precursor protein ($A\beta$ PP)

[5]. The two most common variants of $A\beta$ are 40 or 42 residues long [6–9], and of these two, the 42 residue-version ($A\beta_{42}$) is normally less abundant but more prone to self-aggregate, owing to its longer C-terminus that makes the peptide more hydrophobic [10]. Changes in the amount or form of $A\beta$ in the brain, predominantly involving $A\beta_{42}$, play a decisive role in the development of Alzheimer's disease (AD) [11–13], which is the most common neurodegenerative disease leading to dementia. The onset of AD is

*Correspondence to: Asgeir Kobre-Flatmoen, Olav Kyrres gate 9, 7030 Trondheim, Norway. E-mail: asgeir.kobre-flatmoen@ntnu.no.

characterized by accumulation of intracellular A β_{42} (iA β_{42}), deposits of extracellular amyloid plaques, hyperphosphorylation of the protein tau (p-tau) that subsequently forms neurofibrillary tangles (NFTs), and severe neuronal death. Three of these pathologies, namely accumulation of iA β_{42} , formation of NFTs and severe neuronal death, are predominantly restricted to the medial temporal lobes during the initial stages of the disease. Meanwhile, amyloid plaques tend to arise in neocortical areas [14]. Thus, while A β likely plays a crucial role in the development of AD, neither its physiological role nor its normal expression in neurons is fully understood [15, 16].

A large body of knowledge about AD-pathogenesis comes from the study of rodents made to model aspects of the disease by expressing AD-relevant human transgenes. For example, use of such rodent models established that early changes involving A β_{42} are followed by changes involving p-tau (reviewed in [17]), and that spreading along axonal tracts- and seeding of further pathology is a capacity inherent to both A β [18, 19] and p-tau [20, 21]. A series of experimental results from A β immunization in a transgenic rodent model forming both A β and tau pathology have furthermore shown that, when reducing A β_{42} early on in the pathological cascade, cognitive impairment is reduced or prevented. Once tau-pathology has formed however, reducing A β_{42} is no longer sufficient to prevent cognitive impairment [22, 23]. The latter finding is one that still offers hope for early intervention by A β immunization trials.

While much has come from studying rodent models, it is important to keep in mind that these models of AD are not fully representative of the disease. But it is also important to realize that such models likely do offer a unique window into aspects of pathology at prodromal stages of the disease. We and others [17] therefore believe that rodent models represent opportunities to understand crucial, disease-initiating events, in particular events that involve A β_{42} . It follows that in order to understand what early pathological changes may represent, one must understand the normal condition to which the comparison is made. Yet, when it comes to the normal expression of A β_{42} in rodent brains, surprisingly little is known.

A well-established model for the spatiotemporal onset- and progression of amyloid pathology is the Wistar-based, transgenic McGill-R-Thy1-APP rat model, hereafter referred to as the McGill rat model [24–27]. We therefore decided to characterize the expression of A β_{42} throughout the brain of normal,

outbred Wistar rats, ranging from the time when they are young adults (three months) up to and including relative old age (18 months). We find that iA β_{42} is present in neurons located throughout the brain at all ages of normal Wistar rats, but that the levels vary greatly between brain regions. In cortex, we observe the highest levels of iA β_{42} in neurons that are part of layer II (LII) of the entorhinal cortex (EC), along with neurons in the hippocampus, closely followed by neurons in the somatosensory cortex. Among subcortical structures, we observe the highest levels iA β_{42} in the locus coeruleus. In order to explore whether the striking presence of iA β_{42} also holds true in cognitively intact humans, we examined EC of six cases ranging from ages 20–88. In all six cases, we find that iA β_{42} is present in EC layer II-neurons.

Our findings support two conclusions about iA β_{42} . First, iA β_{42} is present in neurons of wild-type Wistar rats and is restricted to the same structures where iA β accumulates, and A β plaques form, in the McGill AD rat model. The difference between wild-type Wistar rats and McGill model rats, with respect to A β_{42} , is therefore a quantitative one rather than a qualitative one. This indicates that the McGill rat model in fact models the underlying wild-type neuronal population-specific vulnerability to A β_{42} accumulation. Second, because the McGill rat model closely mimics the human AD-associated spatiotemporal sequence of amyloid plaque deposition [27], this model may offer a useful representation of the pre-plaque neuronal accumulation of iA β_{42} . Our findings in human cases are in line with prior findings and substantiate the notion that neurons in layer II of EC are vulnerable to accumulation of iA β_{42} .

METHODS

For this study we used 12 outbred Wistar Han rats. Nine were bred at the Kavli Institute for Systems Neuroscience, originating from a pair purchased from Charles River (France), while three were purchased from Charles River directly. The animals were divided into four age groups, including a 3-month (M) group (two males, one female), a 6 M group (three males), a 12 M group (one male, two females), and an 18 M group (three females). All procedures were approved by the Norwegian Animal Research Authority and follow the European Convention for the Protection of Vertebrate Animals used for Experimental and Other Scientific Purposes. We kept the animals on a 12-h light/dark cycle under standard

laboratory conditions (19–22°C, 50–60% humidity), with access to food and water *ad libitum*. Use of the archival human formalin-fixed postmortem brain tissues was approved by the Ethical review authority (Etikprövningsmyndighetens), Sweden (permit dnr 2021-01609). The human cases, with pathological remarks, include: Case 1, 20-year-old male (no abnormalities mentioned); Case 2, 56-year-old female (no significant abnormalities); Case 3, 64-year-old male (emphysema); Case 4, 73-year-old male (pneumonia); Case 5, 79-year-old male (heart disease); Case 6, 88-year-old male (heart disease).

Processing and immunohistochemistry

Animals were fully anaesthetized by placement in a chamber containing 5% isoflurane gas (Baxter AS, Oslo, Norway) and then given an intraperitoneal injection of pentobarbital (0.1 ml per 100 g; SANIVO PHARMA AS, Oslo, Norway). Transcardial perfusions were carried out with room temperature Ringer's solution (in mM: NaCl, 145; KCl, 3.35; NaHCO₃, 2.38; pH ~6.9) immediately followed by circulation of 4% freshly depolymerized paraformaldehyde (PFA; Merck Life Science AS/Sigma Aldrich Norway AS, Oslo, Norway) in a 125 mM phosphate buffer (PB) solution (VWR International, PA, USA), pH 7.4. The brains were extracted and post-fixed overnight in PFA at 4°C, and then placed in a freeze protective solution (dimethyl sulfoxide in 125 mM PB with 20% glycerol, Merck Life Science AS/Sigma Aldrich Norway AS) until sectioning. Brains were sectioned coronally at 40 µm in six series, using a freezing sledge microtome.

Rat tissue. Immunohistochemistry was done on free-floating sections. To enable optimal access to the antigen the tissue was subjected to gentle heat induced antigen retrieval by placement in PB at 60°C for 2 h. To prevent unspecific labelling the sections were incubated for 2 × 10 min in PB solution containing 3% hydrogen peroxide (Merck Life Science AS/Sigma Aldrich Norway AS), and then incubated for 1 h in PB solution containing 5% normal goat serum (Abcam Cat# ab7481, RRID: AB_2716553). The sections were then incubated with the primary antibody, IBL rabbit anti-Aβ₄₂ (C-terminal specific, from Immuno-Biological Laboratories Cat# JP18582, RRID: AB_2341375) [28, 29], at a 1:500 concentration, in PB containing 0.2% saponin (VWR International AS, Bergen, Norway) for 20 h (overnight). Note that for one animal from each age group, we incubated with the primary anti-

body for approximately 65 h (three days). While this longer incubation time did increase the strength of the signal somewhat, it gave the same pattern of labelling both between and within each brain structure. Next, sections were rinsed for 3 × 5 min in Tris-buffered saline (50 mM Tris, 150 mM NaCl, pH 8.0) containing 0.2% saponin (TBS-Sap), and then incubated with biotinylated secondary antibody goat anti-rabbit (1:400; Sigma-Aldrich Cat#B8895, RRID: AB_258649), in TBS-Sap for 90 min at room temperature. Sections were then rinsed in TBS-Sap, incubated in Avidin-Biotin complex (ABC, Vector Laboratories Cat# PK-4000, RRID: AB_2336818) for 90 min at room temperature, rinsed again, and then incubated in a solution containing 0.67% 3,3'-Diaminobenzidine (Sigma/Merck, Cat# D5905) and 0.024% hydrogen peroxide for 5 min. Sections from animals ranging across the age groups were incubated together in order to safeguard against possible confounds stemming from potentially subtle differences in incubation-time or the quality of the solutions.

Human tissue. Blocks containing EC were embedded in paraffin, sectioned coronally at 8 µm, and mounted on glass slides. Prior to immunohistochemical procedures, the tissue was deparaffinized by immersion in xylene for 5 min × 3 times. The tissue was then rehydrated by being dipped 10 times in water containing decreasing amounts of ethanol (100%, 90%, 70%, 50%, 0%). We blocked against unspecific antigens by applying DAKO Real blocking solution (DAKO, Cat# S2023) for 10 min, followed by application of normal goat serum (same as above) for 1 h. To detect Aβ₄₂, we used the same anti-Aβ₄₂ antibody in the same solution as listed above and incubated the tissue overnight. To also test for the presence or reelin, we used a mouse anti-reelin antibody (Millipore, Cat# MAB5364; RRID:AB_2179313) and carried out double-immunoenzyme labelling. For the anti-Aβ₄₂ antibody we thus used Mach 2 Rabbit HRP Polymer antibody (Biocare Medical, Cat# RHRP520) as our secondary antibody, and visualized it with AEC Red (Sigma-Aldrich, Cat# AEC101). For the anti-reelin antibody, we used a Mach 2 Mouse AP-Polymer (Biocare Medical, Cat# MALP521 G) as secondary antibody, and visualized it with Ferangi Blue Chromogen (Biocare Medical, Cat# BRR813AS). Nissl staining was done by dehydrating sections in ethanol, then clearing in xylene, before rehydration in deionized water and staining with Cresyl violet (1 g/L) for ~5 min. Sections were then alternately dipped in ethanol–acetic acid (5 mL acetic acid in 1 L 70% ethanol) and rinsed with cold water until we obtained

the desired differentiation. The sections were then dehydrated, cleared in xylene and coverslipped with Entellan (Merck KGaA, Darmstadt, Germany).

Processed rat tissue was mounted in Tris-buffered saline on Superfrost Plus slides (Thermo Scientific, Menzel Gäser). A subset of sections was counterstained with Cresyl violet (Nissl-stain). Mounted sections were left to dry overnight and then coverslipped (24 × 60, Thermo Scientific, Menzel Gäser) using a Xylene- (VWR International AS, Bergen, Norway) and Entellan solution (Merck, Darmstadt, Germany). Processed human tissue was left to dry on a heating plate at 37°C for 30 min, and then coverslipped using a water-based medium (Fluoromount-G[®], Southern Biotech, Cat# 0100-01).

Imaging

All rat sections were scanned under identical settings using an automated Zeiss Axio Scan.Z1 system, with a 20x objective (Plan-Apochromat 20x/0.8 M27). The analyses were done in Zen software (2.6, Blue Ed.), based on a qualitative assessment of the intensity of the signal. We divide the intensity of the signal, from here on referred to as the 'level(s)' of A β ₄₂, into five categories: none, denoted -; minimal levels, denoted (+); low-to-moderate levels, denoted +; moderate-to-high levels, denoted ++; and high levels, denoted +++. Representative examples for each level are shown in Fig. 1. Human tissue was inspected using a Zeiss Axio Imager.M1 microscope, and overview images were acquired with this microscope by a MBF Bioscience CX9000 camera using a 10X objective (Zeiss, N.A. 0.45), while insets were acquired using a 20X objective (Zeiss, N.A. 0.8) and a 100X objective (Zeiss, N.A. 1.4 Oil).

RESULTS

To characterize neuronal expression of A β ₄₂ peptides throughout the brain of normal, outbred Wistar rats, we chose an antibody that has previously been shown to be specific against A β ₄₂, namely the IBL A β ₄₂ antibody [29]. For the purpose of validating this antibody also in our hands, we first immunolabeled hippocampal tissue from three-month-old Wistar rats together with hippocampal tissue from 6- and 12-month-old A β PP KO mice [30]. This experiment demonstrates that while there are high levels of iA β ₄₂ immunolabeling in neurons of the CA1-subiculum border region of Wistar rats (see more below), there

is none or only faint background iA β ₄₂ immunolabeling in corresponding neurons (or any other neurons) of A β PP KO mice (Fig. 2; note that there are no A β PP KO rats available). Moreover, for each age-group we took one Wistar rat and ran our immunolabeling protocol on two adjacent sections, where we omitted the primary antibody from one section per age-group while keeping all else identical. From this, it is clear that omitting the primary antibody results in a complete lack of background labelling, i.e., there is no spurious binding of secondary antibodies and/or the chromogen or any associated reagents (Fig. 3). These experiments substantiate the specificity of the antibody.

The following descriptions of our results relate to neuronal somata, unless otherwise specified. Note that since our groups are not gender balanced, we do not address potential sex differences in this study. In broad terms, intracellular A β ₄₂ (iA β ₄₂) is present in neurons found throughout the brain at all ages of normal Wistar rats, but the levels vary greatly between regions, and also within certain regions. We find that as a general tendency, iA β ₄₂ levels increase slightly in wild-type Wistar rats up to and including 12 months of age, before dropping slightly from 12 to 18 months. In the forebrain, we observe the highest levels of iA β ₄₂ in parts of the hippocampus and parts of the entorhinal cortex, followed by the primary somatosensory cortex. In the mid- and hindbrain, we observe the highest levels of iA β ₄₂ in the locus coeruleus and in Purkinje neurons of the cerebellum.

Forebrain

Hippocampal formation (Archicortex). Two gradients of iA β ₄₂ stand out in association with the hippocampal formation. One relates to the transverse axis and involves CA1 and the subiculum, while the other relates to the septotemporal axis and involves the whole hippocampal formation. Relating to the transverse axis, high levels of iA β ₄₂ are present in neuronal somata of the pyramidal layer at the border region between CA1 and the subiculum (CA1/Sub), but the levels of iA β ₄₂ drop when moving away from the CA1/Sub border region. Specifically, in the subiculum, iA β ₄₂ levels are high at the CA1/Sub border region, but this changes to a low-to-intermediate level almost immediately when moving away (distally) from the border region, and remains at this low-to-intermediate level for the remaining distal extent of the subiculum. For CA1, the high iA β ₄₂

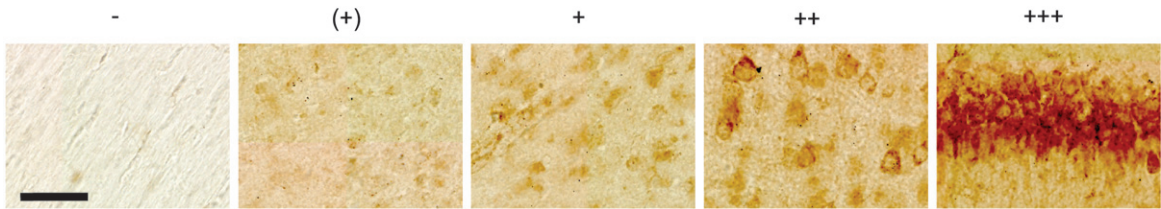


Fig. 1. Representative examples of levels of A β ₄₂ as placed into five different categories, including none (denoted -), minimal levels (denoted +), low-to-moderate levels (denoted +), moderate-to-high levels (denoted ++), and high levels (denoted +++). These examples are taken from a 12-month-old animal. Scale bar = 50 μ m.

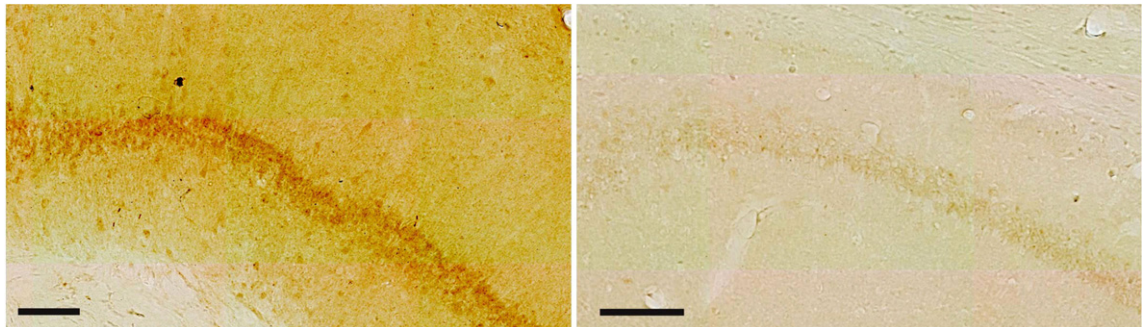


Fig. 2. The A β ₄₂ antibody is specific: (left image) Immunolabeling with the IBL A β ₄₂ antibody reveals a high level of signal in CA1 of three-month-old Wistar rats, while (right image) practically no signal is present in CA1 of 6-month-old APP-Knockout mice (same results were obtained for 12-month-old APP-Knockout mice). Scale bars = 100 μ m. Images were acquired using identical settings.

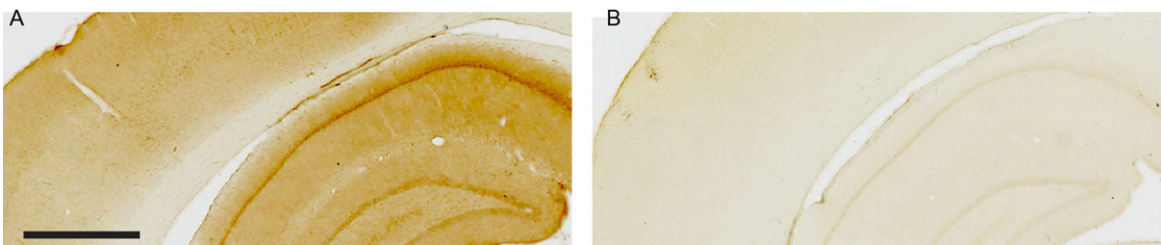


Fig. 3. Omission of the anti-A β ₄₂ primary antibody demonstrates lack of background labeling. A) Part of neocortex and the dorsal hippocampus after three-day incubation with anti-A β ₄₂ primary antibody followed by visualization with 3,3'-Diaminobenzidine as the chromogen (see Methods for details). B) Adjacent section undergoing identical treatment but where the anti-A β ₄₂ primary antibody was omitted. Sections are from an 18-month-old Wistar rat. Scale bar: (A) = 1000 μ m as also applies to (B).

levels at the CA1/Sub border region extend into approximately the distal half of CA1. From this point, iA β ₄₂ levels gradually drop as one moves successively further away from the CA1/Sub border region, such that at the proximal extreme of CA1, iA β ₄₂ levels are low (Fig. 4A). Meanwhile, the gradient relating to the septotemporal axis, which holds true for all the hippocampal fields (DG, CA1-CA3, and Sub), is such that each field has higher levels of iA β ₄₂ in their septal domain *relative to* their temporal domain. While both the transverse and the septotemporal gradient is consistently present across animals, the absolute levels of iA β ₄₂ vary between animals.

This between-animal variation is most notable for DG and CA3. Specifically, in some animals the iA β ₄₂ levels in DG and CA3 come close to, though not quite reaching that seen for the CA1/Sub border region, while for other animals the iA β ₄₂ levels in DG and CA3 are substantially lower than that for the CA1/Sub border region (Fig. 4B).

The most clearly observable iA β ₄₂ signal is generally restricted to somata with our immunohistochemical method, but CA1 pyramidal neurons constitute an exception in that many show iA β ₄₂ also in their basal dendrites, extending into stratum radiatum. Another feature of CA1 is that iA β ₄₂ levels are

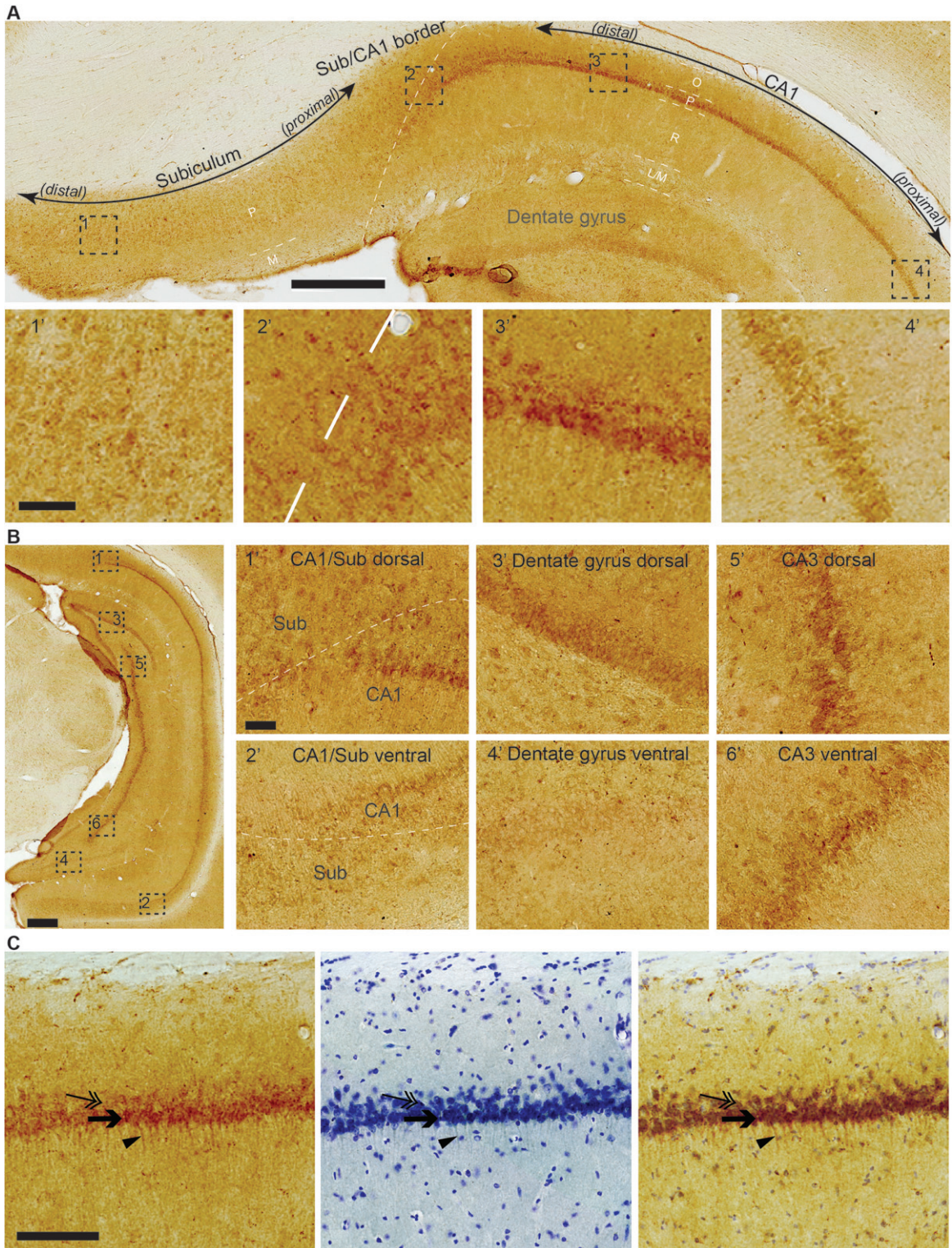


Fig. 4. (Continued)

noticeably higher in neurons situated in the superficial part of the pyramidal layer; most of the dendritic iA β ₄₂ seems to be associated with these superficially situated neurons (Fig. 4C).

Piriform cortex (Archicortex). In the piriform cortex, a far greater number of neurons in layer II stain positive for iA β ₄₂ than neurons in layer III. Most neurons have moderate iA β ₄₂ levels, though a few neurons have moderate-to-high levels. Neuropil-labelling is generally low, except in the outer half of layer I, where a moderate A β ₄₂ positive band of labelling is present (Fig. 5A, B).

Parahippocampal region (Periallocortex). In the lateral entorhinal cortex (LEC), the population of large fan neurons that are situated in the superficial part of layer II and close to the rhinal fissure, is one of the few neuronal populations whose somata contain high levels of iA β ₄₂ in the normal rat brain. When moving successively further away from the rhinal fissure, the levels of iA β ₄₂ in fan neurons gradually drop, reaching the lowest levels at the point furthest away from the rhinal fissure (Fig. 6A). This is different for the medial entorhinal cortex (MEC), where LII contains so-called stellate neurons, which are considered a counterpart population of neurons to the LEC fan-neurons (for more details on properties and differences between LII-neurons in LEC versus MEC, please see the following papers [31, 32]). Thus, while a similar gradient to that described for LEC is present also in MEC, with higher levels of iA β ₄₂ being present in stellate neurons close to the rhinal fissure, the total levels of iA β ₄₂ in MEC stellate neurons are generally far less than for LEC fan neurons (Fig. 6B). However, we observe a notable between-animal variation with respect to iA β ₄₂ in MEC, with occasional animals having moderate-to-high levels in stellate neurons close to the rhinal fissure.

In LEC LIII, and to a lesser degree in MEC LIII, neurons close to the rhinal fissure have moderate-to-high levels of iA β ₄₂. Though less pronounced than that for LII, there is a similar gradient vis-a-vis the rhinal fissure, such that neurons located increasingly further away from the rhinal fissure express less iA β ₄₂. We do not observe such a gradient for neuronal somata in deeper layers, where the levels of iA β ₄₂ range from low-to-moderate (Fig. 6A, B).

For the remaining structures that make up the parahippocampal region, namely the pre- and parasubiculum, and the peri- and postrhinal cortices, we find that iA β ₄₂ levels range from low-to-moderate. In the pre- and parasubiculum, low levels tend to dominate in deeper layers while moderate levels tend to dominate in superficial layers. In the perirhinal cortex, the ventrally situated area 35 tends to have low levels of iA β ₄₂ across the layers, while the dorsally situated area 36 tends to have low levels in the superficial layers and low-to-moderate levels in the deeper layers. In the postrhinal cortex, iA β ₄₂ levels are low-to-moderate, with layers II and V-VI tending towards moderate levels, and layer III tending towards low levels.

Neocortex (Allocortex). A majority of neurons in most areas of the neocortex have low or minimal levels of iA β ₄₂. An exception to this general finding is the primary somatosensory cortex, and to a lesser extent the primary motor cortex. The primary somatosensory cortex harbors a great number of neurons with moderate-to-high levels of iA β ₄₂ across layers II-VI, of which those with the highest levels constitute pyramidal neurons in layer V. In the adjacent primary motor cortex, low-to-moderate iA β ₄₂ levels are present in layers II-V, while low levels are present in layer VI (Fig. 7A-C). Low or

Fig. 4. A) Top micrograph: High levels of iA β ₄₂ are present in neuronal somata of the pyramidal layer at the border region between CA1 and the subiculum (distal CA1, proximal subiculum), but iA β ₄₂ levels diminish in intensity when moving away from this border region, such that low levels of iA β ₄₂ are present in proximal CA1 and distal subiculum. For the subiculum, the decrease in iA β ₄₂ levels occurs almost immediately distal to the CA1/subiculum border region, while for CA1, the decrease occurs more gradually when moving increasingly proximal from this border region. Dashed white line indicates border between CA1 and the subiculum. Layers are indicated by short dashed white line and white text for CA1 and Sub: O, Oriens; P, Pyramidale; R, Radiatum; L/M, Lacunosum/Moleculare; M, Moleculare. Bottom micrographs: Higher-powered insets taken from top micrograph, numbers according to location. B) Leftmost micrograph: Hippocampal formation at the maximal dorsoventral extent achieved by a coronal section. Right-side insets: iA β ₄₂ levels are substantially higher in the dorsal than in the ventral portion of the hippocampal formation. Notice the moderate-to-high levels of iA β ₄₂ in dorsal dentate gyrus and dorsal CA3 in this example; this feature is variable between animals. Insets numbered according to location. Dashed white line in 1' and 2' indicates the border between CA1 and the subiculum. C) Rightmost micrograph: In CA1, superficially located pyramidal neurons have higher levels of iA β ₄₂ (arrow) than those located deeper (double-arrow), and many of those superficially located CA1 pyramidal neurons have iA β ₄₂ extending into their basal dendrites (arrowhead). Middle micrograph: Nissl stain of adjacent section (Cresyl Violet). Rightmost micrograph: iA β ₄₂- and Nissl-stained sections-overlay. Data are from an 18-month-old animal. Scale bars: (A and B) top micrograph 500 μ m, bottom micrographs, 50 μ m, (C) 200 μ m.

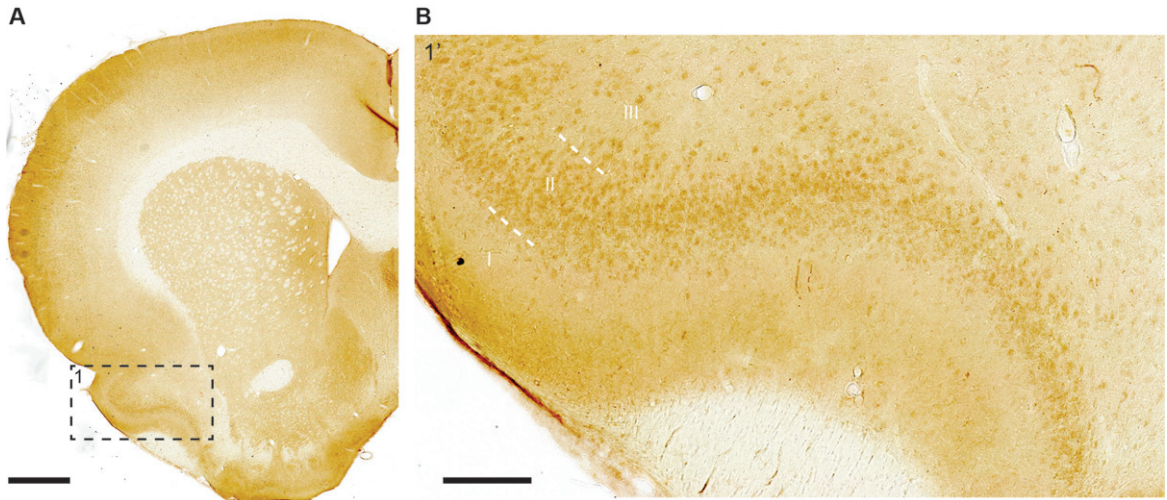


Fig. 5. Moderate-to-high levels of $iA\beta_{42}$, mainly leaning towards moderate, are present in layer II neurons of the piriform cortex. A far lesser number of layer III neurons also stain positive for $iA\beta_{42}$. A) Frontal section with example of piriform cortex indicated (1, dashed rectangle), along with (B) higher-powered inset. Note that aside from the signal in neurons, an $A\beta_{42}$ -positive band of labelling is present in the outer half of layer I. Scale bars: (A) 1000 μm , (B) 200 μm .

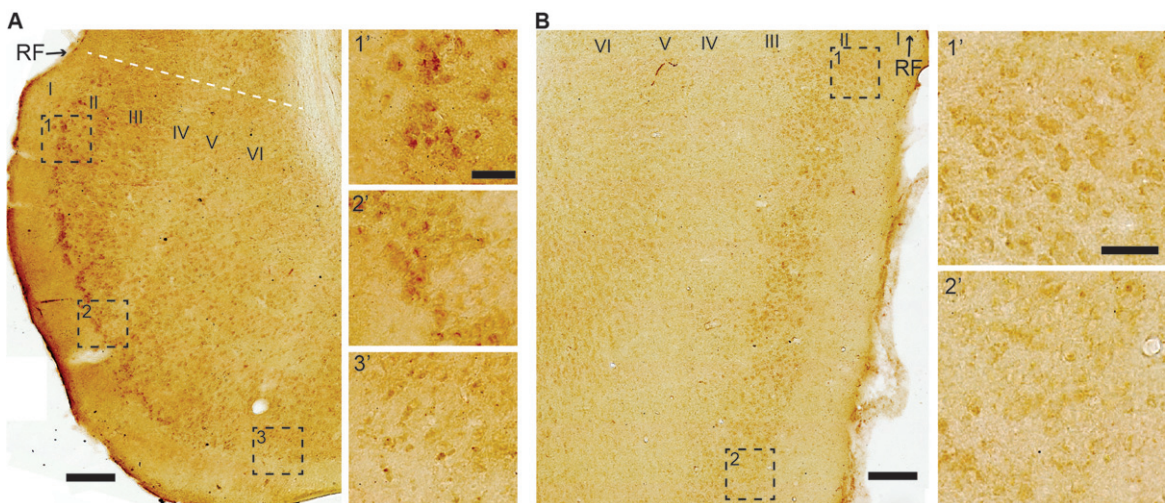


Fig. 6. High levels of $iA\beta_{42}$ are present in entorhinal cortex (EC) LII-neurons that are situated close to the rhinal fissure. A) In LEC, high levels of $iA\beta_{42}$ are present in neurons in the outer portion of LII that are close to the rhinal fissure (RF); $iA\beta_{42}$ levels gradually diminish in intensity when moving successively further away from RF, being reduced to low levels at the point furthest away from RF. This feature is similar, though less pronounced, also in the case of LIII, but is not present in deeper layers. B) In MEC, low-to-moderate levels of $iA\beta_{42}$ are present in LII neurons located close to RF, and, similar to that of LEC, $iA\beta_{42}$ levels diminish in intensity when moving successively further away from the rhinal fissure. Layers are indicated (I-VI). Dashed white line in (A) indicates border with perirhinal cortex. Micrographs are from an 18-month-old animal. Scale bars 200 μm and insets 50 μm .

low-to-moderate levels of $iA\beta_{42}$ are present also in many layer V pyramidal neurons of the secondary motor cortex and the parietal association cortex; in both of the latter cortices, a lesser number of layer V pyramidal neurons have moderate-to-high $iA\beta_{42}$ levels.

Mid- and hindbrain

In the mid- and hindbrain, levels of $iA\beta_{42}$ are generally minimal. However, striking exceptions to this general finding include the cerebellum, and the locus coeruleus of the brainstem.

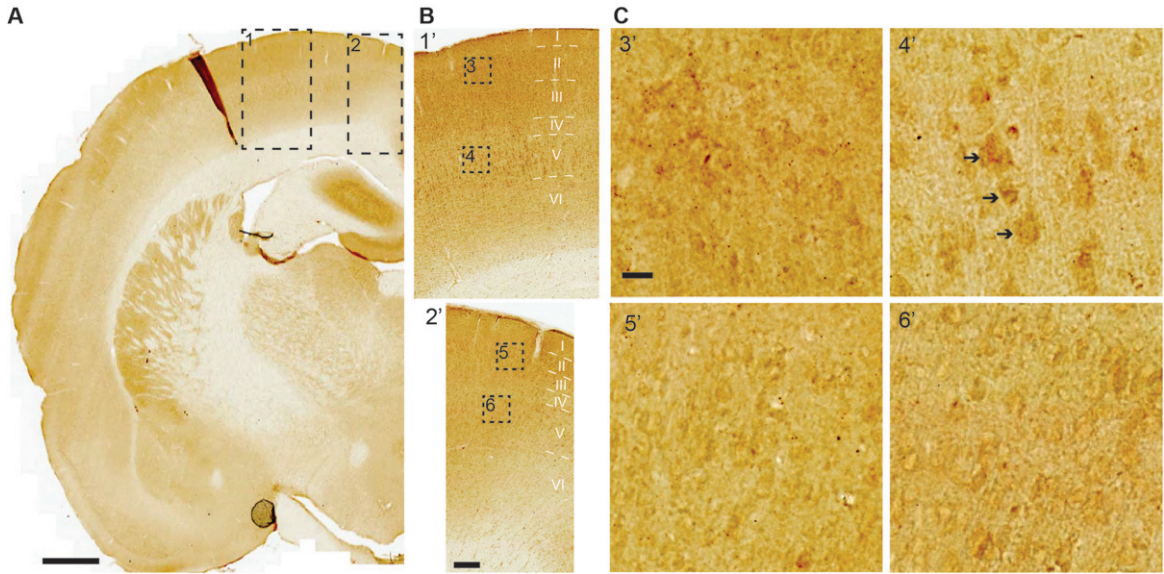


Fig. 7. Moderate-to-high levels $iA\beta_{42}$ are present in the primary somatosensory cortex, most notably in layer V. A) Levels of $iA\beta_{42}$ are generally low across the neocortex. But in the primary somatosensory cortex (dashed rectangle 1), moderate-to-high $iA\beta_{42}$ levels are present in layer V pyramidal neurons, and low-to-moderate levels of $iA\beta_{42}$ are present in neurons of superficial layers along with layer VI. In the adjacent primary motor cortex (dashed rectangle 2), low-to-moderate $iA\beta_{42}$ levels are present in layers II-V, while low levels are present in layer VI. B, C) Increasingly higher-powered insets; note the examples of clearly stained layer V pyramidal neurons (arrows) in primary somatosensory cortex (inset 4'). Scale bars: (A) 1000 μm , (B) 200 μm , (C) 20 μm .

Cerebellum. Most neurons in the cerebellum have no detectable or minimal levels of $iA\beta_{42}$. Purkinje neurons constitute an exception as these have high levels of $iA\beta_{42}$ and thus stand out in striking contrast to the cerebellar granule neurons (Fig. 8). We do not observe any clear gradient with respect to the distribution of $iA\beta_{42}$ levels between Purkinje neurons of different portions in the cerebellum.

Locus coeruleus. In the locus coeruleus, we find high levels of $iA\beta_{42}$ in neurons located in the very densely packed dorsomedial portion (Fig. 9). A Nissl counterstain reveals that these neurons are round or ovoid, which corresponds to previously published findings about the morphology of neurons in this portion of the locus coeruleus [33].

Human entorhinal cortex

Based on our findings in normal rats, together with multiple lines of evidence showing that accumulation of $iA\beta_{42}$, formation of NFTs and severe neuronal death arises in EC-layer II already at the initial stages of AD, we sought to examine sections of EC from human subjects free of neurological disease. We examined six such cases, ranging from 20–88 years of age. From each human case we immunolabeled sections of EC using the same $iA\beta_{42}$ antibody

as that for rats. Similar to our findings in the normal rat brain, we find that $iA\beta_{42}$ is present in EC layer II-neurons in all six human control cases (Fig. 10A-C). Furthermore, the intensity of $iA\beta_{42}$ labeling was greater in older subjects relative to younger ones. In order to answer whether $A\beta_{42}$ was located inside EC layer II-neurons also in the oldest case, where some of the $A\beta_{42}$ labeling started to take on the appearance of small plaques, we counterstained a section with cresyl violet. This revealed that, in many cases, a nucleus and a nucleolus was still situated inside the $A\beta_{42}$ labeling (Fig. 10C).

DISCUSSION

A generic criticism against transgenic rodent models for AD is that they typically have “non-physiological expression” of their transgenic product or that they fail to form pathology in the correct brain structure [34]. Given that they constitute the vast majority of AD models, it is certainly relevant to address such criticism with respect to rodent models expressing mutant human $A\beta$ PP to cause increased levels of $A\beta$ ($A\beta$ PP models). While with the development of AD, $A\beta$ levels are no longer physiological, which is what rodent $A\beta$ PP models model, it is crucial to know whether a given transgene expresses in the

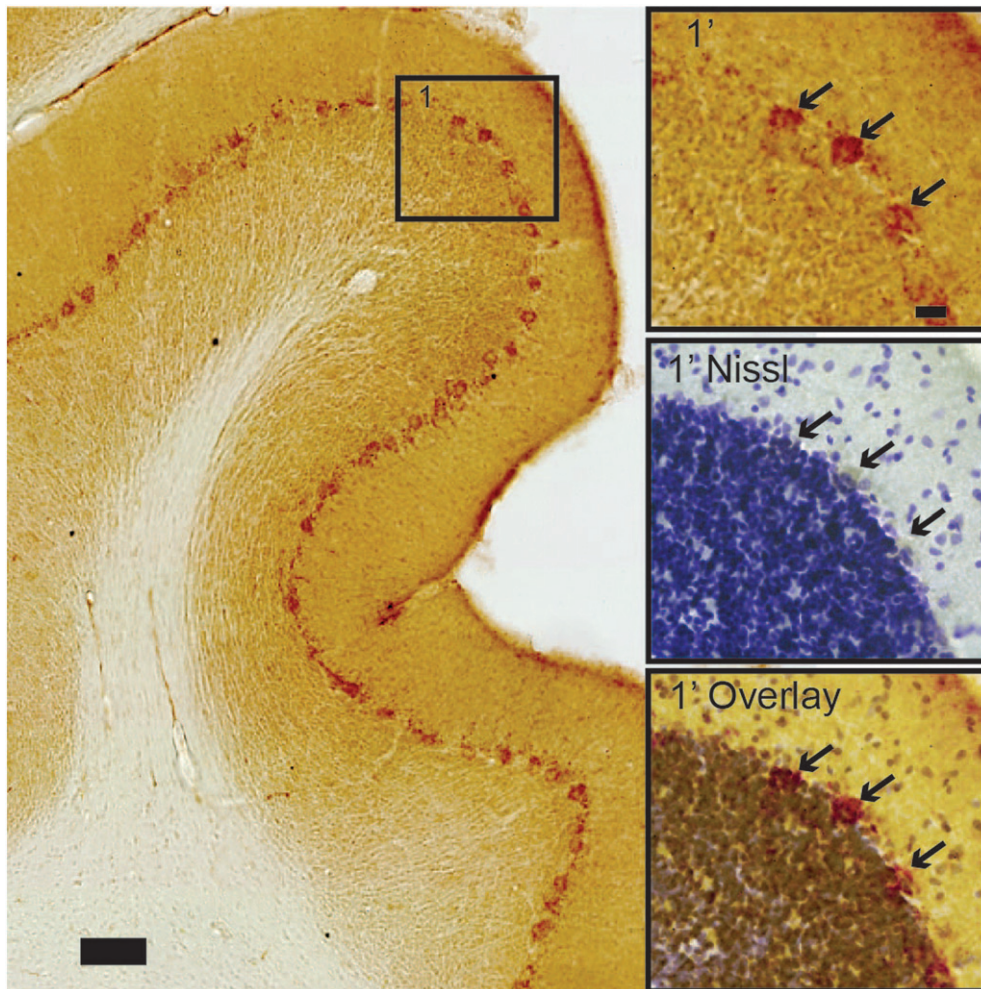


Fig. 8. Cerebellar Purkinje neurons contain high levels of $iA\beta_{42}$, in stark contrast to surrounding neurons. Insets show arrows pointing to (top) $iA\beta_{42}$ -positive Purkinje neurons, followed by (middle) the position of these neurons after Nissl counterstain on the same section, and (bottom) a contrast enhanced overlay of the top and middle insets. Scale bars: 100 μm (large image) and insets 20 μm .

relevant brain structures, but also whether the given transgene causes increased expression of its protein product in structures that ought not to be affected. Yet, while recent work used healthy rats to look at certain proteins capable of forming amyloids (i.e., fibrillar aggregates) [35], little is known about the normal, brain structure-specific expression of $A\beta$ in rodents. Here we characterized the brain-wide presence of $iA\beta_{42}$ in normal outbred Wistar rats. This rat strain forms the background-strain for the much-used McGill rat model [24], an $A\beta\text{PP}$ model that mimics the spatiotemporal sequence of amyloid plaque deposition seen in human AD subjects [27] and has an extended pre-plaque period of $iA\beta$ accumulation [26].

We find that in normal wild-type Wistar rats, neurons in a subset of structures involving both the forebrain and the hindbrain express surprisingly high levels of $iA\beta_{42}$. These structures include the part of LEC LII located close to the rhinal fissure, the CA1/Sub border region, and the somatosensory cortex (forebrain), along with the cerebellum and the locus coeruleus (hindbrain). With respect to the forebrain, these relatively high $iA\beta_{42}$ -expressing structures are the exact structures in which amyloid plaque pathology first arise in the transgenic mutated $hA\beta\text{PP}$ -based McGill rat model [27]. In particular, plaque-pathology in the McGill rat model begins in the proximal portion of the subiculum and typically also involves the distal part of CA1 (see

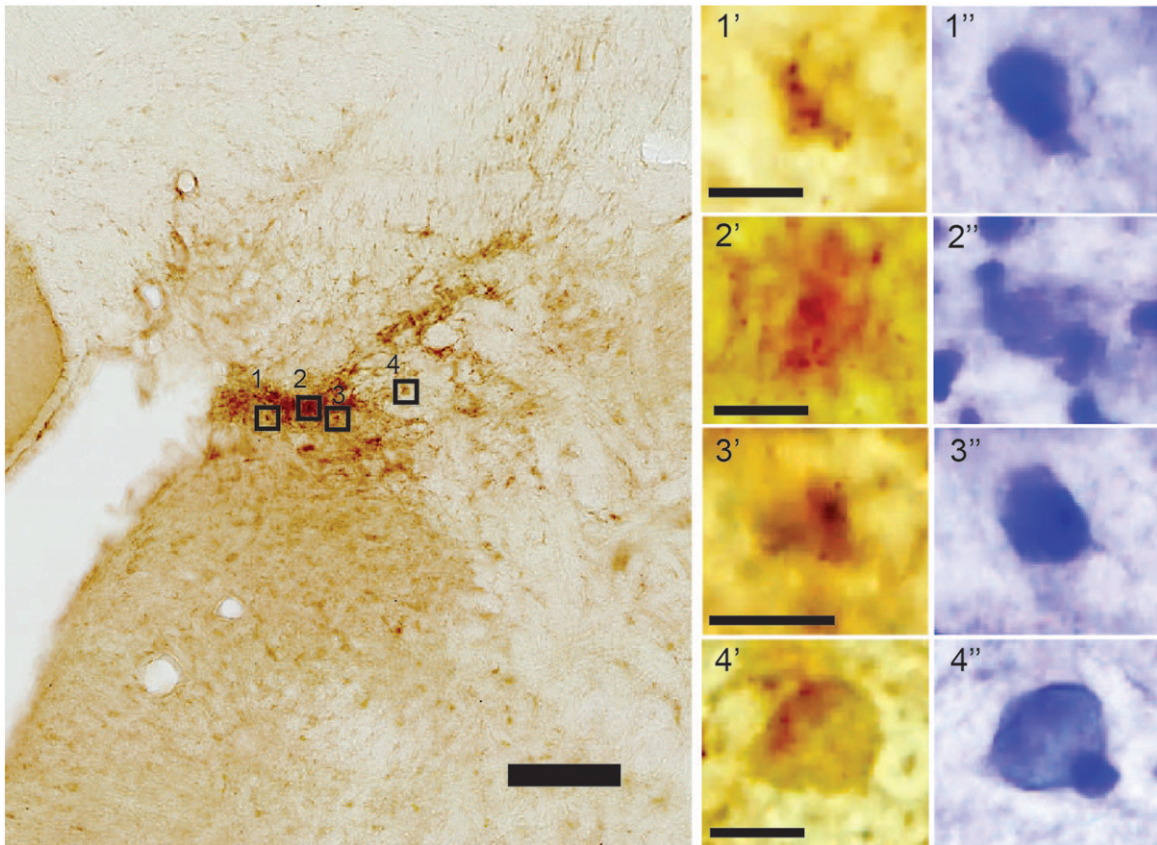


Fig. 9. High levels of $iA\beta_{42}$ in cells of the dorsomedial part of the locus coeruleus. A Nissl counterstain done on top of the DAB-labeled section (insets) reveals that several of these cells are round or ovoid. Note that at this portion of the locus coeruleus the cells are very densely packed, and contrast enhancement was necessary to separate adjacent cells. Scale bars: 100 μm (large image) and insets 10 μm .

Fig. 12L&M in [27]), thus perfectly matching the portion of the hippocampus where, relative to other areas, high levels of endogenous $iA\beta_{42}$ are present in normal Wistar rats. Subsequent to the CA1/Sub, plaques in the McGill model deposit in the part of LEC located close to the rhinal fissure (see Figs. 14O and 16O in [27]), again matching the substructure where we find a particularly high level of endogenous $iA\beta_{42}$ in normal Wistar rats. The same is the case for the neocortex, as the McGill model deposits its first *neocortical* plaques in the somatosensory- and motor cortex, which is the only part of the neocortex in which we find a high level of endogenous neuronal $iA\beta_{42}$ in normal Wistar rats.

We are not aware of any available data regarding the hindbrain of the McGill rat model. Nevertheless, our findings that cerebellar Purkinje neurons and neurons in the locus coeruleus in normal Wistar rats selectively express high levels of $iA\beta_{42}$ are

of considerable interest. It is well known that amyloid plaques eventually form in the cerebellum in AD [36], and such plaques have been linked specifically to $A\beta$ -laden Purkinje neurons [37]. It is notable in this context that even though NFTs do not seem to readily form in the cerebellum, this might depend on the $A\beta_{42}$ load, since at least one type of familial AD (PS1-E280A), caused by increased production of $A\beta_{42}$, leads to formation of cerebellar p-tau [38]. Contrary to this, the locus coeruleus is, alongside laterally situated entorhinal layer II-neurons, particularly prone to early formation of p-tau and formation of NFTs [39]. While little is known regarding the possibility of $A\beta$ accumulating in the locus coeruleus during the pre-clinical phase of AD, a recent study using an antibody against oligomeric or fibrillar $A\beta$ on cases with full-blown AD did report the presence of plaques in the locus coeruleus [40]. A major question in the field is how $A\beta$ induces tau

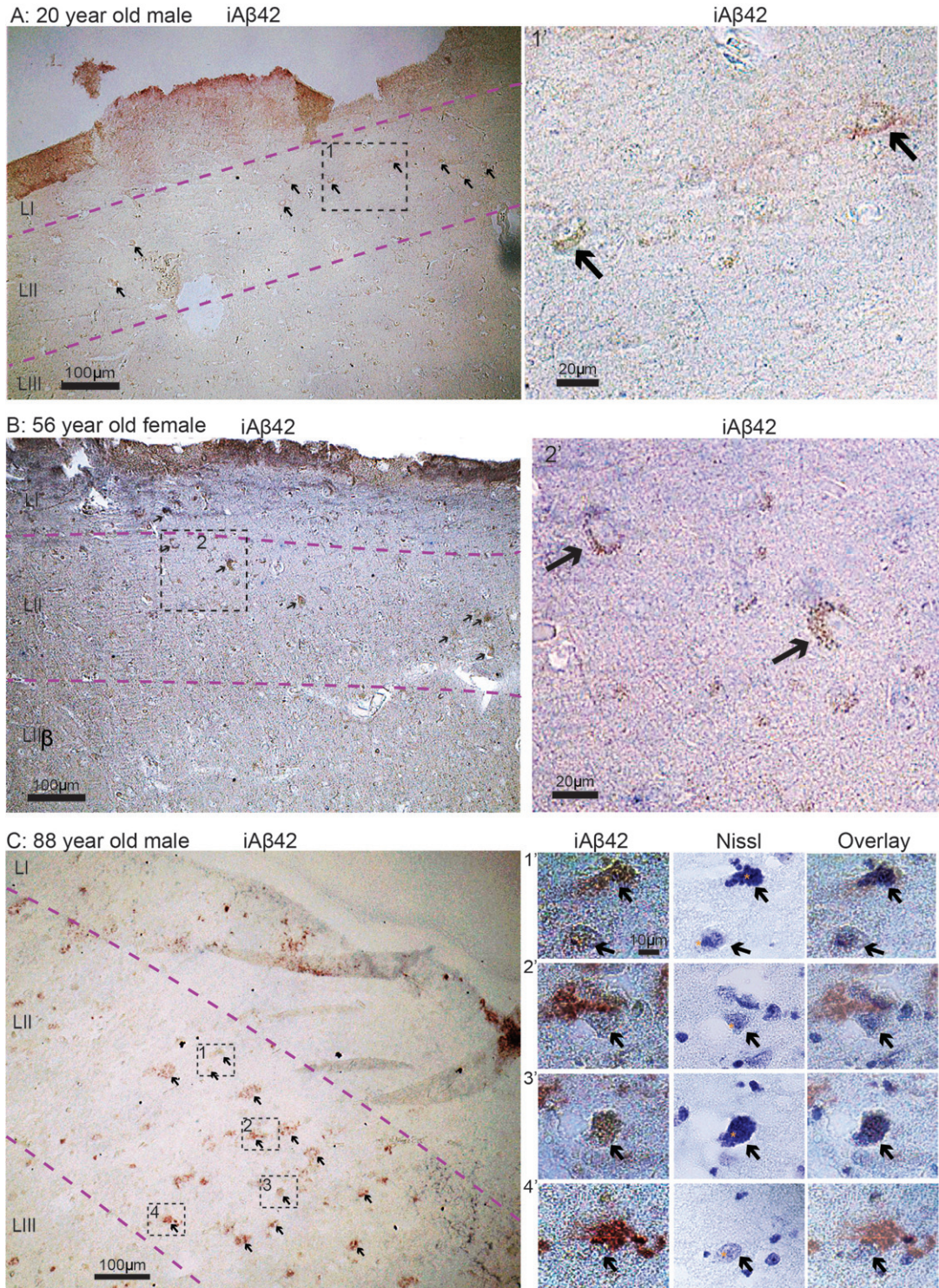


Fig. 10. iA β ₄₂ is present in entorhinal cortex layer II neurons in human subjects free of neurological disease. A) 20-year-old male. B) 56-year-old female. C) 88-year-old male. Overview images in (A-C) were taken with a 10x objective, insets for (A) and (B) were taken with a 20x objective, while insets for (C) were taken with a 100x oil immersion objective. Immunolabelling and Nissl staining is indicated for each image/panel. Stippled lines in light magenta indicate layers. To indicate nucleoli in the middle panels of (C), we have placed a small asterisk immediately to the left of each. Scale bars are indicated for each image/panel (in (C), the scale bar in top left image applies to all in this panel).

pathology. The location of i β inside neurons could more directly lead to effects on tau kinases, thereby inducing pathological tau phosphorylation [41] and subsequent tangle pathology. Of note, it has been shown that i β_{42} precedes antibody AT8 positive phospho-tau in human EC LII neurons [42] and CA1 pyramidal neurons [43].

To provide some human correlate to our findings in normal Wistar rats to human brains we also carried out β_{42} immunolabeling on EC-tissue from six cases of cognitively normal human subjects, ranging from 20–88 years of age. In all six cases, we find i β_{42} in EC layer II-neurons, substantiating prior findings in humans about the vulnerability of such neurons to accumulate β [26, 43–45]. Why the somata of such EC layer II-neurons (or EC layer II in itself) are not associated with plaque formation in AD remains unclear, although our working hypothesis is that the i β_{42} in somata of EC layer II neurons then shifts to their axon terminals in the perforant pathway, which develop prominent β_{42} aggregation [18].

β is produced naturally by neurons. Our findings in normal Wistar rats that certain neurons express more i β_{42} , like for example those in part of LEC LII and in the CA1/Sub border region, therefore ties in with ongoing efforts to elucidate the normal role of β peptides. Current evidence to various degrees supports several possibilities, including that β may suppress microbial activity, help repair brain injuries, promote the sealing of a leaky blood-brain barrier, and/or that it regulates synaptic plasticity [46]. Of these, at least the latter notion is relevant with respect to our present results, since the neurons in which we find the highest expression of i β_{42} are in structures associated with high activity levels, including LEC LII [47], the hippocampus [48], and the somatosensory cortex [49]. Indeed, levels of neuronal activity have been found to correlate with levels of β as long as the latter are within normal levels (reviewed in [46]).

Because the structures with the most notable expression of neuronal i β_{42} in normal Wistar rats are the same as those which show early neuronal i β_{42} in the McGill rat model, and because this rat model closely mimics the AD-related spatiotemporal cascade of AD neuron vulnerability and β plaque deposition [27], we conclude that it is well suited for the purpose of modelling the cascade of amyloid pathology seen in the context of AD. We emphasize that this likely includes the pre-plaque neuronal accumulation of i β_{42} , which in the McGill rat model extends over approximately 8 months.

ACKNOWLEDGMENTS

We wish to thank Bruno Monterotti, Hanne Tegner Soligard, Paulo Jorge Bettencourt Girão, and Grethe Mari Olsen for excellent technical assistance.

FUNDING

This work was funded by The Olav Thon Foundation, The K. G. Jebsen Centre for Alzheimer's Disease, and The Norwegian Research Council Centre of Excellence Grant.

CONFLICT OF INTEREST

The authors have no conflict of interest to report.

DATA AVAILABILITY

Raw data will be made available upon request.

REFERENCES

- [1] Gouras GK, Almeida CG, Takahashi RH (2005) Intraneuronal Abeta accumulation and origin of plaques in Alzheimer's disease. *Neurobiol Aging* **26**, 1235-1244.
- [2] Naslund J, Haroutunian V, Mohs R, Davis KL, Davies P, Greengard P, Buxbaum JD (2000) Correlation between elevated levels of amyloid beta-peptide in the brain and cognitive decline. *JAMA* **283**, 1571-1577.
- [3] Wertkin AM, Turner RS, Pleasure SJ, Golde TE, Younkin SG, Trojanowski JQ, Lee VM (1993) Human neurons derived from a teratocarcinoma cell line express solely the 695-amino acid amyloid precursor protein and produce intracellular beta-amyloid or A4 peptides. *Proc Natl Acad Sci U S A* **90**, 9513-9517.
- [4] Haass C, Schlossmacher MG, Hung AY, Vigo-Pelfrey C, Mellon A, Ostaszewski BL, Lieberburg I, Koo EH, Schenk D, Teplow DB, Selkoe DJ (1992) Amyloid beta-peptide is produced by cultured cells during normal metabolism. *Nature* **359**, 322-325.
- [5] Steiner H, Fukumori A, Tagami S, Okochi M (2018) Making the final cut: Pathogenic amyloid-beta peptide generation by gamma-secretase. *Cell Stress* **2**, 292-310.
- [6] Perez RG, Soriano S, Hayes JD, Ostaszewski B, Xia W, Selkoe DJ, Chen X, Stokin GB, Koo EH (1999) Mutagenesis identifies new signals for beta-amyloid precursor protein endocytosis, turnover, and the generation of secreted fragments, including Abeta42. *J Biol Chem* **274**, 18851-18856.
- [7] Koo EH, Squazzo SL (1994) Evidence that production and release of amyloid beta-protein involves the endocytic pathway. *J Biol Chem* **269**, 17386-17389.
- [8] Jarrett JT, Berger EP, Lansbury Jr PT (1993) The carboxy terminus of the beta amyloid protein is critical for the seeding of amyloid formation: Implications for the pathogenesis of Alzheimer's disease. *Biochemistry* **32**, 4693-4697.
- [9] Busciglio J, Gabuzda DH, Matsudaira P, Yankner BA (1993) Generation of beta-amyloid in the secretory pathway in neuronal and nonneuronal cells. *Proc Natl Acad Sci U S A* **90**, 2092-2096.

- [10] Chromy BA, Nowak RJ, Lambert MP, Viola KL, Chang L, Velasco PT, Jones BW, Fernandez SJ, Lacor PN, Horowitz P, Finch CE, Krafft GA, Klein WL (2003) Self-assembly of A β 1-42 into globular neurotoxins. *Biochemistry* **42**, 12749-12760.
- [11] Pereira JB, Janelidze S, Ossenkoppele R, Kvartsberg H, Brinkmalm A, Mattsson-Carlgrén N, Stomrud E, Smith R, Zetterberg H, Blennow K, Hansson O (2021) Untangling the association of amyloid-beta and tau with synaptic and axonal loss in Alzheimer's disease. *Brain* **144**, 310-324.
- [12] Mattsson-Carlgrén N, Andersson E, Janelidze S, Ossenkoppele R, Insel P, Strandberg O, Zetterberg H, Rosen HJ, Rabinovici G, Chai X, Blennow K, Dage JL, Stomrud E, Smith R, Palmqvist S, Hansson O (2020) Abeta deposition is associated with increases in soluble and phosphorylated tau that precede a positive Tau PET in Alzheimer's disease. *Sci Adv* **6**, eaaz2387.
- [13] Jonsson T, Atwal JK, Steinberg S, Snaedal J, Jonsson PV, Bjornsson S, Stefansson H, Sulem P, Gudbjartsson D, Maloney J, Hoyte K, Gustafson A, Liu Y, Lu Y, Bhargale T, Graham RR, Huttenlocher J, Bjornsdottir G, Andreassen OA, Jonsson EG, Palotie A, Behrens TW, Magnusson OT, Kong A, Thorsteinsdottir U, Watts RJ, Stefansson K (2012) A mutation in APP protects against Alzheimer's disease and age-related cognitive decline. *Nature* **488**, 96-99.
- [14] Palmqvist S, Scholl M, Strandberg O, Mattsson N, Stomrud E, Zetterberg H, Blennow K, Landau S, Jagust W, Hansson O (2017) Earliest accumulation of beta-amyloid occurs within the default-mode network and concurrently affects brain connectivity. *Nat Commun* **8**, 1214.
- [15] Galanis C, Fellenz M, Becker D, Bold C, Lichtenthaler SF, Müller UC, Deller T, Vlachos A (2021) Amyloid-beta mediates homeostatic synaptic plasticity. *J Neurosci* **41**, 5157-5172.
- [16] Huang L, McClatchy DB, Maher P, Liang Z, Diedrich JK, Soriano-Castell D, Goldberg J, Shokhirev M, Yates JR, 3rd, Schubert D, Currais A (2020) Intracellular amyloid toxicity induces oxytosis/ferroptosis regulated cell death. *Cell Death Dis* **11**, 828.
- [17] Zahs KR, Ashe KH (2010) 'Too much good news' - are Alzheimer mouse models trying to tell us how to prevent, not cure, Alzheimer's disease? *Trends Neurosci* **33**, 381-389.
- [18] Roos TT, Garcia MG, Martinsson I, Mabrouk R, Israelsson B, Deierborg T, Kobro-Flatmoen A, Tanila H, Gouras GK (2021) Neuronal spreading and plaque induction of intracellular Abeta and its disruption of Abeta homeostasis. *Acta Neuropathol* **142**, 669-687.
- [19] Kane MD, Lipinski WJ, Callahan MJ, Bian F, Durham RA, Schwarz RD, Roher AE, Walker LC (2000) Evidence for seeding of beta -amyloid by intracerebral infusion of Alzheimer brain extracts in beta-amyloid precursor protein-transgenic mice. *J Neurosci* **20**, 3606-3611.
- [20] Iba M, Guo JL, McBride JD, Zhang B, Trojanowski JQ, Lee VM (2013) Synthetic tau fibrils mediate transmission of neurofibrillary tangles in a transgenic mouse model of Alzheimer's-like tauopathy. *J Neurosci* **33**, 1024-1037.
- [21] Liu L, Drouet V, Wu JW, Witter MP, Small SA, Clelland C, Duff K (2012) Trans-synaptic spread of tau pathology in vivo. *PLoS One* **7**, e31302.
- [22] Oddo S, Caccamo A, Tran L, Lambert MP, Glabe CG, Klein WL, LaFerla FM (2006) Temporal profile of amyloid-beta (Abeta) oligomerization in an *in vivo* model of Alzheimer disease. A link between Abeta and tau pathology. *J Biol Chem* **281**, 1599-1604.
- [23] Billings LM, Oddo S, Green KN, McLaugh JL, LaFerla FM (2005) Intraneuronal Abeta causes the onset of early Alzheimer's disease-related cognitive deficits in transgenic mice. *Neuron* **45**, 675-688.
- [24] Leon WC, Canneva F, Partridge V, Allard S, Ferretti MT, DeWilde A, Vercauteren F, Atifeh R, Ducatenzeiler A, Klein W, Szyf M, Alhonen L, Cuello AC (2010) A novel transgenic rat model with a full Alzheimer's-like amyloid pathology displays pre-plaque intracellular amyloid-beta-associated cognitive impairment. *J Alzheimers Dis* **20**, 113-126.
- [25] Sosulina L, Mittag M, Geis HR, Hoffmann K, Klyubin I, Qi Y, Steffen J, Friedrichs D, Henneberg N, Fuhrmann F, Justus D, Keppler K, Cuello AC, Rowan MJ, Fuhrmann M, Remy S (2021) Hippocampal hyperactivity in a rat model of Alzheimer's disease. *J Neurochem* **157**, 2128-2144.
- [26] Kobro-Flatmoen A, Nagelhus A, Witter MP (2016) Reelin-immunoreactive neurons in entorhinal cortex layer II selectively express intracellular amyloid in early Alzheimer's disease. *Neurobiol Dis* **93**, 172-183.
- [27] Heggland I, Storkaas IS, Soligard HT, Kobro-Flatmoen A, Witter MP (2015) Stereological estimation of neuron number and plaque load in the hippocampal region of a transgenic rat model of Alzheimer's disease. *Eur J Neurosci* **41**, 1245-1262.
- [28] Kretner B, Trambauer J, Fukumori A, Mielke J, Kuhn PH, Kremmer E, Giese A, Lichtenthaler SF, Haass C, Arzberger T, Steiner H (2016) Generation and deposition of Abeta43 by the virtually inactive presenilin-1 L435F mutant contradicts the presenilin loss-of-function hypothesis of Alzheimer's disease. *EMBO Mol Med* **8**, 458-465.
- [29] Saito T, Suemoto T, Brouwers N, Sleegers K, Funamoto S, Mihira N, Matsuba Y, Yamada K, Nilsson P, Takano J, Nishimura M, Iwata N, Van Broeckhoven C, Ihara Y, Saito TC (2011) Potent amyloidogenicity and pathogenicity of Abeta43. *Nat Neurosci* **14**, 1023-1032.
- [30] Zheng H, Jiang M, Trumbauer ME, Sirinathsinghi DJ, Hopkins R, Smith DW, Heavens RP, Dawson GR, Boyce S, Conner MW, Stevens KA, Slunt HH, Sisoda SS, Chen HY, Van der Ploeg LH (1995) beta-Amyloid precursor protein-deficient mice show reactive gliosis and decreased locomotor activity. *Cell* **81**, 525-531.
- [31] Canto CB, Witter MP (2012) Cellular properties of principal neurons in the rat entorhinal cortex. I. The lateral entorhinal cortex. *Hippocampus* **22**, 1256-1276.
- [32] Canto CB, Witter MP (2012) Cellular properties of principal neurons in the rat entorhinal cortex. II. The medial entorhinal cortex. *Hippocampus* **22**, 1277-1299.
- [33] Wilcox BJ, Unnerstall JR (1990) Identification of a subpopulation of neuropeptide Y-containing locus coeruleus neurons that project to the entorhinal cortex. *Synapse* **6**, 284-291.
- [34] Drummond E, Wisniewski T (2017) Alzheimer's disease: Experimental models and reality. *Acta Neuropathol* **133**, 155-175.
- [35] Chirinskaite AV, Siniukova VA, Velizhanina ME, Sopova JV, Belashova TA, Zadorsky SP (2021) STXBP1 forms amyloid-like aggregates in rat brain and demonstrates amyloid properties in bacterial expression system. *Prión* **15**, 29-36.
- [36] Braak H, Braak E, Bohl J, Lang W (1989) Alzheimer's disease: Amyloid plaques in the cerebellum. *J Neurol Sci* **93**, 277-287.
- [37] Wang HY, D'Andrea MR, Nagele RG (2002) Cerebellar diffuse amyloid plaques are derived from dendritic Abeta42

- accumulations in Purkinje cells. *Neurobiol Aging* **23**, 213-223.
- [38] Sepulveda-Falla D, Matschke J, Bernreuther C, Hagele C, Puig B, Villegas A, Garcia G, Zea J, Gomez-Mancilla B, Ferrer I, Lopera F, Glatzel M (2011) Deposition of hyperphosphorylated tau in cerebellum of PS1 E280A Alzheimer's disease. *Brain Pathol* **21**, 452-463.
- [39] Braak H, Thal DR, Ghebremedhin E, Del Tredici K (2011) Stages of the pathologic process in Alzheimer disease: Age categories from 1 to 100 years. *J Neuropathol Exp Neurol* **70**, 960-969.
- [40] Kelly L, Seifi M, Ma R, Mitchell SJ, Rudolph U, Viola KL, Klein WL, Lambert JJ, Swinny JD (2021) Identification of intraneuronal amyloid beta oligomers in locus coeruleus neurons of Alzheimer's patients and their potential impact on inhibitory neurotransmitter receptors and neuronal excitability. *Neuropathol Appl Neurobiol* **47**, 488-505.
- [41] Willen K, Edgar JR, Hasegawa T, Tanaka N, Futter CE, Gouras GK (2017) Abeta accumulation causes MVB enlargement and is modelled by dominant negative VPS4A. *Mol Neurodegener* **12**, 61.
- [42] Welikovitsh LA, Do Carmo S, Magloczky Z, Szocsics P, Loke J, Freund T, Cuello AC (2018) Evidence of intraneuronal Abeta accumulation preceding tau pathology in the entorhinal cortex. *Acta Neuropathol* **136**, 901-917.
- [43] Gouras GK, Tsai J, Naslund J, Vincent B, Edgar M, Checler F, Greenfield JP, Haroutunian V, Buxbaum JD, Xu H, Greengard P, Relkin NR (2000) Intraneuronal Abeta42 accumulation in human brain. *Am J Pathol* **156**, 15-20.
- [44] D'Andrea MR, Nagele RG, Wang HY, Lee DH (2002) Consistent immunohistochemical detection of intracellular beta-amyloid42 in pyramidal neurons of Alzheimer's disease entorhinal cortex. *Neurosci Lett* **333**, 163-166.
- [45] D'Andrea MR, Nagele RG, Wang HY, Peterson PA, Lee DH (2001) Evidence that neurones accumulating amyloid can undergo lysis to form amyloid plaques in Alzheimer's disease. *Histopathology* **38**, 120-134.
- [46] Jeong H, Shin H, Hong S, Kim Y (2022) Physiological roles of monomeric amyloid-beta and implications for Alzheimer's disease therapeutics. *Exp Neurobiol* **31**, 65-88.
- [47] Hevner RF, Wong-Riley MT (1992) Entorhinal cortex of the human, monkey, and rat: Metabolic map as revealed by cytochrome oxidase. *J Comp Neurol* **326**, 451-469.
- [48] Cheng X, Vinokurov AY, Zherebtsov EA, Stelmashchuk OA, Angelova PR, Esteras N, Abramov AY (2021) Variability of mitochondrial energy balance across brain regions. *J Neurochem* **157**, 1234-1243.
- [49] Hevner RF, Liu S, Wong-Riley MT (1995) A metabolic map of cytochrome oxidase in the rat brain: Histochemical, densitometric and biochemical studies. *Neuroscience* **65**, 313-342.